Marine Pollution Bulletin 97 (2015) 160–168

Contents lists available at ScienceDirect

Marine Pollution Bulletin

journal homepage: www.elsevier.com/locate/marpolbul

# Tracking the origins of plastic debris across the Coral Sea: A case study from the Ouvéa Island, New Caledonia

Christophe Maes *, Bruno Blanke

*Laboratoire de Physique des Océans, UMR 6523 CNRS-Ifremer-IRD-UBO, Centre Ifremer de Brest, ZI de la Pointe du Diable, 29280 Plouzané, France*
*UFR Sciences et Techniques, 6 avenue Le Gorgeu, CS 93837, 29238 Brest CEDEX 03, France*

ARTICLE INFO

*Article history:*
Received 27 February 2015
Revised 10 June 2015
Accepted 11 June 2015
Available online 16 June 2015

*Keywords:*
Plastic debris pollution
Southwestern Pacific
Coral Sea circulation
Lagrangian dispersion
Meridional drift pathways
Transfer times

ABSTRACT

Contamination of the marine environment by human-made plastic litter is a growing and global problem. Our study attempts to explain the presence of two plastic bottles beached on the Ouvéa Island, in the southwest Pacific Ocean, with trademarks from the Solomon Islands and Papua New Guinea (PNG). We simulate the oceanic drift tracks and associated transit times with a Lagrangian interpretation of the surface currents of a high-resolution ocean model. Our results show that it takes less than 2–3 months for drifting objects to connect these archipelagos (New Caledonia, Solomon Islands and PNG) and highlight the role of the meridional component of the circulation rather than the dominant zonal jets. This study shows that the origin or traceability of trash represent valuable information that can be used to test and, ultimately, improve our understanding of ocean circulation.



## 1. Introduction

Since the pioneering study by Capenter and Smith (1972) of the plastic debris in the Sargasso Sea, the pollution of the marine environment by discarded plastic has come to be recognized as a global problem and a major threat to marine life (e.g., Depledge et al., 2013). In a recent study by Eriksen et al. (2014) it was estimated that more than 5 trillion pieces of plastic are floating on the surface across large areas such as the subtropical gyres of the global ocean as well as marginal seas such as the Bay of Bengal and the Mediterranean Sea. The wide distribution of plastic debris and its accumulation in marginal bays, gulfs and seas suggests that ocean currents play an important role in this phenomenon, connecting widely separated regions across basins. A famous example is the dispersion of the Fukushima debris across the North Pacific following the massive tsunami of March 2011 (Bailly du Bois et al., 2014). Less spectacular perhaps than the Fukushima example, but as important, is the concentration of debris in the center of the gyres by the surface convergence such as studied in the South Pacific Ocean by Martinez et al. (2009).

Model predictions of where pollutants or debris might disperse or converge gained renewed attention in recent years by the use of global and regional mappings of the ocean surface's mesoscale motion derived from satellite missions (indirect products taking advantage of combined altimetry and surface wind stress) or by considering probabilistic models of dispersion based on trajectories reported by surface drifters or numerical models (Dohan and Maximenko, 2010; Maximenko et al., 2012; Sudre et al., 2013; Froyland et al., 2014). If such approaches shed light on the strength of the connectivity between the different regions of the ocean, the surface circulation always reveals still more complex patterns that vary on multiple spatial and temporal scales. Therefore, it is crucial to fully understand the connections between the different modes of climate variability and the accumulation and dispersal of debris. In such a context, it is useful to take advantage of direct reports of marine debris on shorelines as data points to test our ability to simulate their dispersion and routes across the oceans.

The direct observations reported in this study originate from cruises operated in the context of the SPICE program (Ganachaud et al., 2014), which is focused the inflow of the South Equatorial Current (SEC) into the Coral and Solomon Seas, in the southwest Pacific Ocean (Fig. 1). In order to estimate the ocean circulation and the mass balance in the region, several cruises were staged to conduct transects between islands. During the transit of the Bifurcation cruise between New Caledonia and the Chesterfield Islands in September 2012, five hydrographic stations were supplemented by water samples to be examined for the presence of micro-plastics. The results revealed very low levels of

* Corresponding author at: LPO, Centre Ifremer de Brest, ZI de la Pointe du Diable, CS 10070, 29280 Plouzané, France.
*E-mail address:* christophe.maes@ird.fr (C. Maes).

http://dx.doi.org/10.1016/j.marpolbul.2015.06.022
0025-326X/

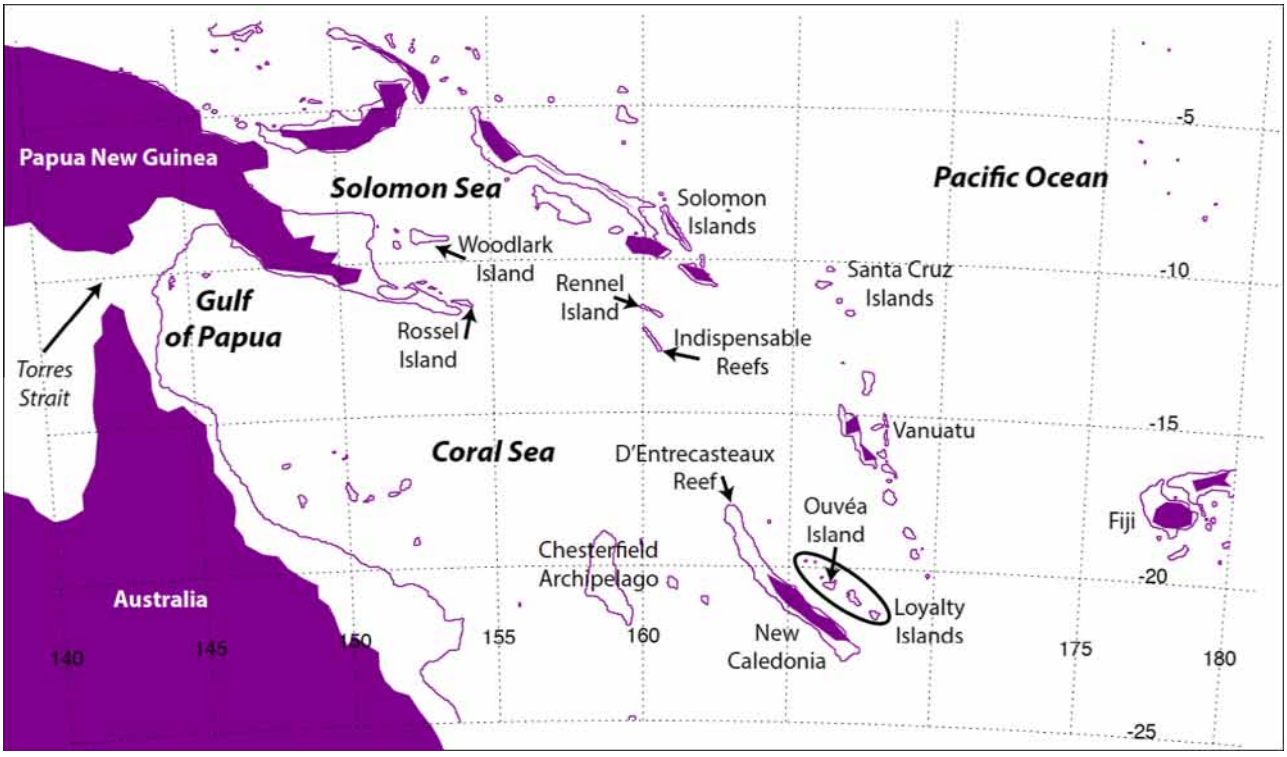


**Fig. 1.** Area of study and place names used in the text. The land filled in purple shows the continental boundaries of our visualization software whereas the purple line refers to the actual mask of the NLOM surface velocity. (For interpretation of the references to color in this figure legend, the reader is referred to the web version of this article.)

micro-plastics at these stations, with one station having no particles at all (M. Henry and F. Galgani, pers. comm.). This can be explained both by the low density of the human population in this region and by the presence of many sandy islands and reefs where macro-plastics are beached before they can be degraded by mechanical abrasion and chemical weathering.

Nevertheless on a number of these cruises we noted the presence of plastic and marine debris on the beaches at several locations such as the Chesterfield Islands (20°S–159°E), the sandy Surprise islet of the D'Entrecasteaux reef at the tip of New Caledonia (18°S–163°E) and the Ouvéa Island (20.5°S–166.5°E (Fig. 2a), which is one of the major Loyalty Islands located to the east of New Caledonia. It was only at the last site that we found two plastic bottles that were in relatively good shape and could be identified as originating from the Solomon Islands and Papua New Guinea (PNG) (Fig. 2b). These bottles were found on the beach of Ouvéa on November 11, 2011. This beach is exposed directly to the ocean on the east side of the island where the outside reef barrier is less than 50 m from the beach (red circle in Fig. 2a). The foreign origin of these bottles was counter to our expectation that the majority of debris at this site is generated locally and counter as well to the fact that the general organization of the mean surface ocean circulation is dominated by zonal jets and westward currents directed toward the Australian coast (Choukroun et al., 2010). Discounting other possible distant and local origins for these bottles (the region is visited by commercial vessels navigating between the various archipelagos of the Coral Sea), we took as the major objective of this study to examine the possibility that their primary source was as labeled on the bottles: the Solomon Islands and PNG. To this end we considered the potential of meridional currents to transport floating macro-plastic litter such as these bottles over long distances. Special attention was paid to the transfer time required to travel from these sources to the beach at Ouvéa Island.

## 2. Ocean model and Lagrangian method

### 2.1. NLOM velocity data

For this study, we used daily surface zonal and meridional velocity components from the Naval Research Laboratory (NRL) Layered Ocean Model (hereafter NLOM) run at 1/32° horizontal resolution for the period 2010–2011. The model strengths lie in its very fine grid resolution and in the incremental updating technique used to assimilate sea surface height and sea surface temperature data (Shriver et al., 2007). The results of this global nowcast system are currently distributed by the Asia–Pacific Data-Research Center (APDRC) of the International Pacific Research Center located in Honolulu, Hawaii. We extracted the velocity data for our region of interest in the western tropical Pacific, from 140°E to 180°E and from 25°S to 2°S (Fig. 1).

A few missing dates (calendar days 95, 111, 116, 250 and 342 of 2010 and calendar days 38, 83 and 254 of 2011) and a few missing latitudes between 7.25°S and 2.94°S on day 223 of 2010 were replaced by linear interpolation of data for the days before and after.

### 2.2. Model assessment

A thorough validation of the model surface velocity field is beyond the scope of our study. However, we checked that the mean currents from the NLOM data were consistent with previous descriptions of the surface circulation entering into the Coral Sea. To this end we remapped the 2010–2011 average of the NLOM currents to a resolution of roughly 1/3° with the result shown in Fig. 3. Following the study by Webb (2000) and further discussion by Kessler and Gourdeau (2007) in their analysis of another ocean model, we were able to identify unambiguously the major jets in the region: the North and South Fiji Jets (NFJ and SFJ), the North

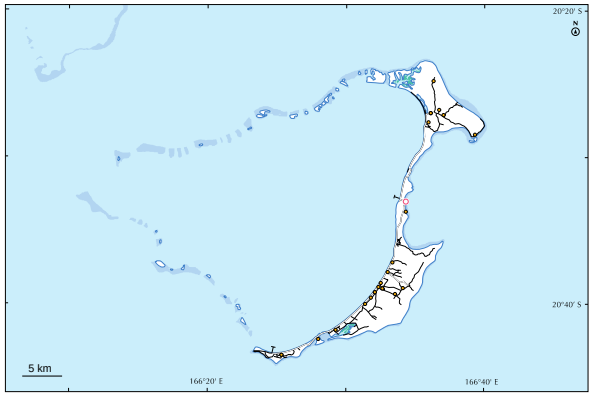


**Fig. 2.** (a) Detailed map of the Ouvéa Island with the position of the collection site (red circle) and (b) photograph of the two plastic bottles on which can be seen their countries of production. (For interpretation of the references to color in this figure legend, the reader is referred to the web version of this article.)

and South Caledonia Jets (NCJ and SCJ) and the North Vanuatu Jet (NVJ). The surface boundary currents were also identifiable in this annual mean, specifically the equatorward Gulf of Papua Current (GPC) and the southward East Australia Current (EAC) along the Australian coast after their bifurcation on the Queensland plateau. The GPC is associated with a large transport of thermocline waters around a very sharp bend (Gasparin et al., 2012) as it enters the Solomon Sea to form the New Guinea Coastal Undercurrent (NGCU) at the tip of PNG at Rossel Island. North of the domain, the intense westward flowing SEC and the eastward flowing South Equatorial Counter Current (SECC) dominate the northern boundary of our area of interest. All of these features are also, in their general path and magnitude, coherent with the observed regional circulation deduced from ship mounted current meters and Lagrangian surface drifter data. These direct observations also show that the circulation in the region is characterized by a high degree of variability at seasonal and interannual timescales (Cravatte et al., 2011; Hristova and Kessler, 2012). In the following, in order to match the expected timeframe for the drift of the plastic bottles, only the model currents for the 2010–2011 period will be considered.

Zonal flows dominate in the Coral Sea with multiple jets. Yet, of interest here is the presence of significant meridional currents, flowing southward in addition to the EAC on the flanks of Australia. These southward flows appear as part of the recirculation in the lee of Rennel Island and the Indispensable reefs (near 12°S–158°E), as a southeastward flow along the Solomon Islands that connects with the SECC in the Pacific Ocean, and as the dominant southward flow connecting the NVJ and the NCJ in the region between Vanuatu and New Caledonia. This last feature is also present in a surface current climatology derived from the surface drifters (R. Lumpkin, pers. comm.). We will return to the drifter data in Section 3.3 for an assessment of transit times deduced from locally available drifters.

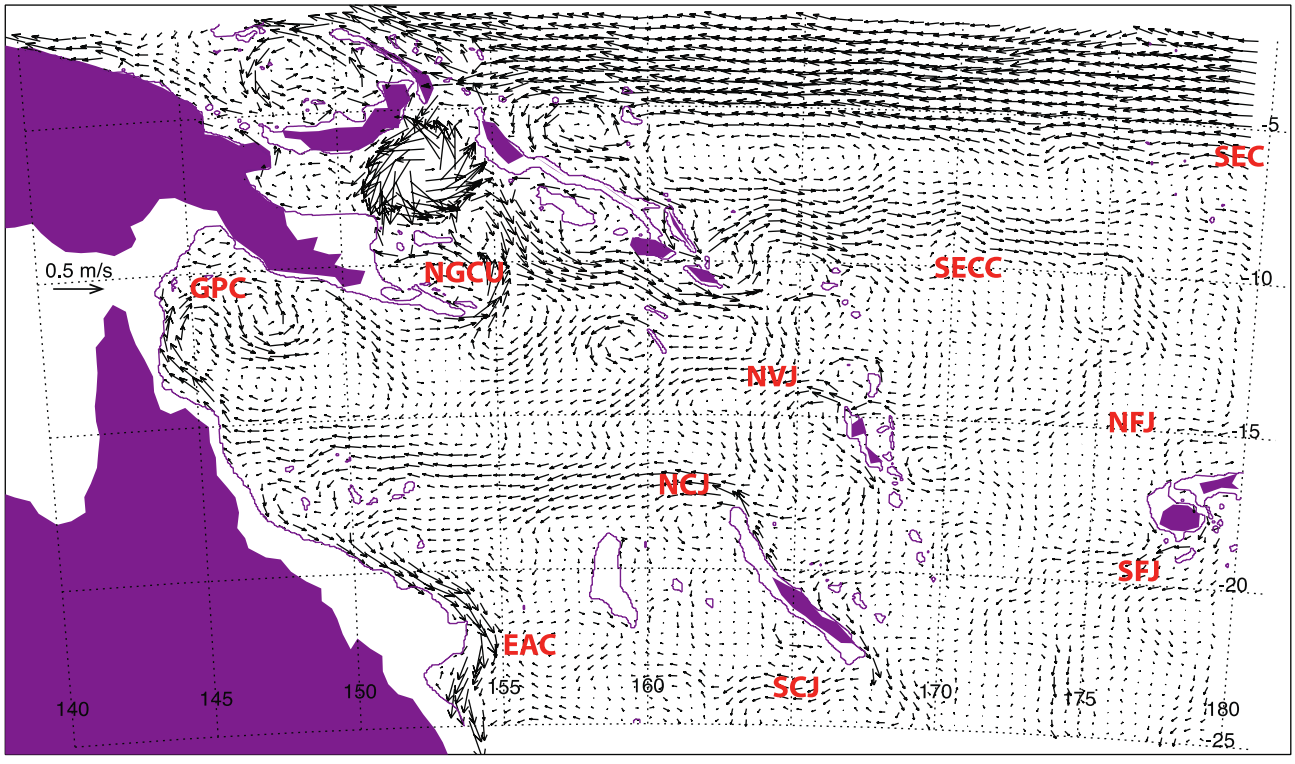


**Fig. 3.** Model surface circulation averaged over 2010–2011 and interpolated on a 1/3° stencil. Major jets and currents are identified with the acronyms specified in the text.

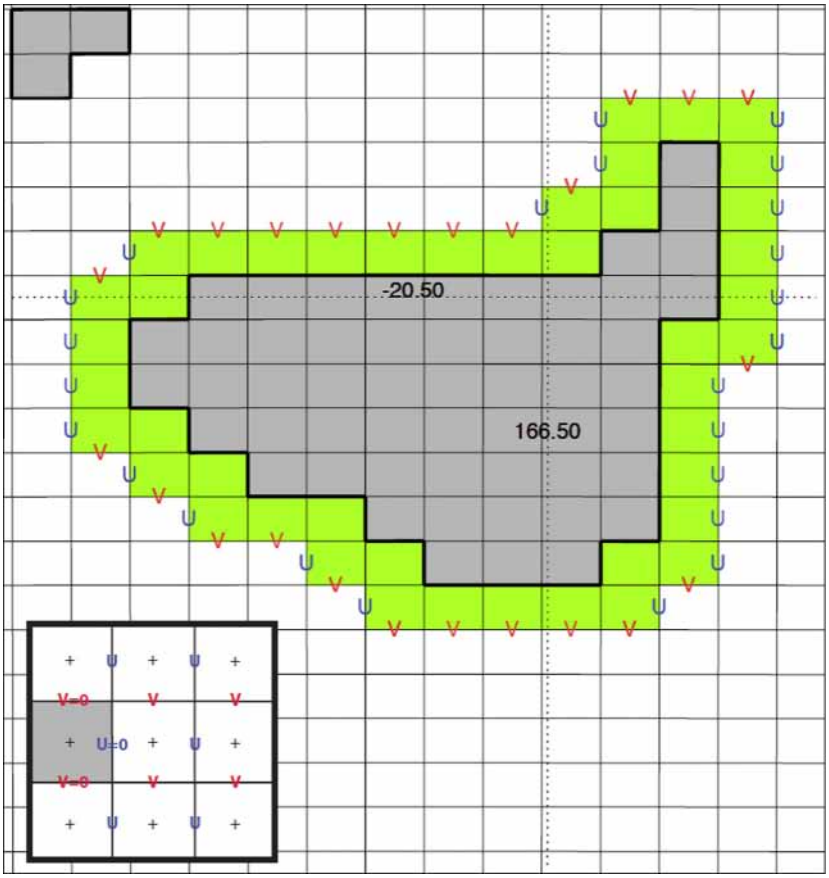


**Fig. 4.** Initialization strategy around Ouvéa Island. The initial section is defined as the edge of the first belt of ocean grid cells (green shading) surrounding the mask (gray shading) of the full atoll. Note that the island itself is a simple crescent located over the eastern part of the area filled in gray. The particles are distributed along the zonal and meridional sides of the grid cells facing the open ocean, and they are associated with a weight equal to a fraction of the transport inferred from the local zonal or meridional velocity component (multiplied by the width of the grid cell and by an arbitrary 10-m thickness). The trajectories being integrated backward in time, only the U and V grid points showing movement toward the coast are considered in the initialization process. In the bottom left, the insert shows the preparation of the horizontal velocity components for Ariane calculations. The original positions of both components of the NLOM surface velocity field are shown with "plus" signs. The positions of the zonal and meridional components of the velocity field interpolated on the Ariane C grid are given in blue and red, respectively. Undefined NLOM velocity data define a "land" grid cell in the C grid (gray shading), and the velocity components on its sides are forced to zero. (For interpretation of the references to color in this figure legend, the reader is referred to the web version of this article.)

While the mean circulation is important to consider in this study, a large part of the Lagrangian transport in the ocean is associated with mesoscale eddies and submesoscale features such as filaments and fronts. We compared the average kinetic energy in the model with the equivalent derived from the purely geostrophic velocity components produced by Segment Sol Multimissions d'Altimétrie, d'Orbitographie et de Localisation Précise/Data Unification and Altimeter Combination System (SSALTO/DUACS) and distributed by Archiving, Validation, and Interpretation of Satellite Oceanographic data (AVISO). The calculation was done for 2010 and for the oceanic box extending from 154°E to 164°E and from 18°S to 12°S, i.e., the eastern part of the Coral Sea. The total kinetic energy of the surface velocity field was averaged over this domain and was separated into mean and variable components. The kinetic energy computation, based on the geostrophic velocity from the delayed-time daily altimetry at 1/4° horizontal resolution, showed total, mean and turbulent kinetic energy values of 0.063, 0.011 and 0.052 $m^2\ s^{-2}$, respectively. More than 80% of the total kinetic energy in this calculation stemmed from perturbations of the mean flow. This proportion was the same for the calculation based on the NLOM surface velocity field, but with a total kinetic energy 25% larger; the breakdown here was 0.083, 0.016 and 0.067 $m^2\ s^{-2}$, respectively. The ageostrophic processes in the model and its finer grid resolution allowed for a significant increase in both the mean and turbulent flows. These ageostrophic currents are essential in Lagrangian calculations of realistic trajectories.

### 2.3. Trajectory calculations

The trajectory calculations were made with Ariane, a Lagrangian toolkit that has demonstrated its utility for tracing water mass movements in the output of ocean general circulation models (http://www.univ-brest.fr/lpo/ariane; Blanke and Raynaud, 1997; Blanke et al., 1999). The Lagrangian calculations were 2D in space, with no allowance for vertical movement. Since Ariane works on a staggered C-grid (Arakawa, 1972), we interpolated the velocity components either zonally (for U) or meridionally (for V), keeping the land/ocean mask of NLOM as the mask used in the Ariane calculations (Fig. 4). The velocity grid points of the C grid located on the sides of a masked grid cell are set to zero to prevent trajectory forays into masked grid cells. The grid parameters needed for operating Ariane (geographical coordinates and scale factors) are derived from the original longitudes and latitudes of the NLOM velocity components.

The pathways from the southern Gulf of Papua, PNG and the Solomon Islands to Ouvéa Island were studied by means of backward Lagrangian calculations from the coastal ocean around

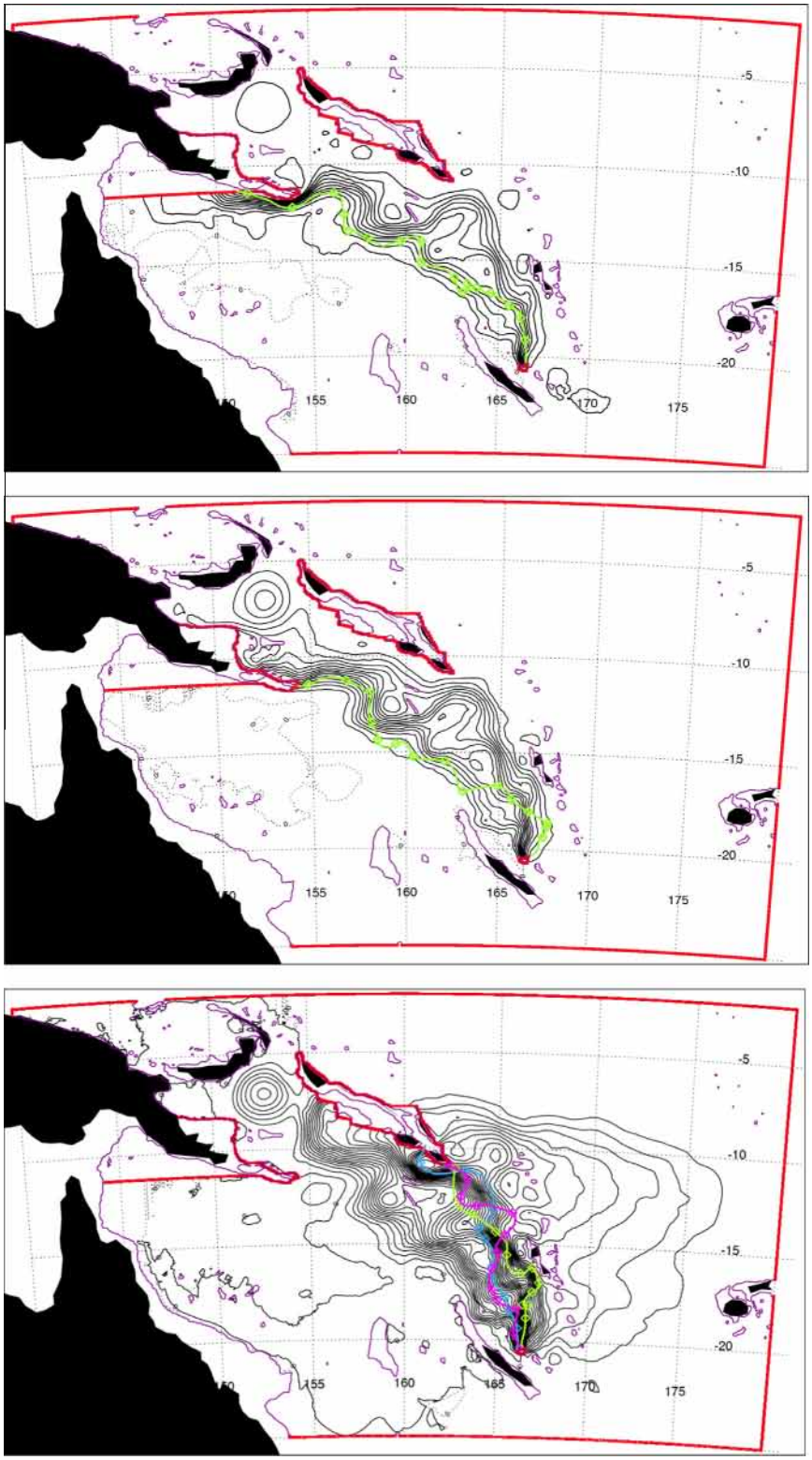


**Fig. 5.** Lagrangian stream functions for the connections calculated to Ouvéa Island. (a) From the Solomon Islands. (b) From the eastern tip of Papua New Guinea. (c) From the southern Gulf of Papua. The contour interval is 10 $m^2/s$ and the value of the stream function is arbitrarily set to 0 over Australia. The whole set of control sections is drawn in red, knowing that the mask derived from the NLOM surface velocity is an impenetrable barrier for the particles (purple line). Since the formal derivation of the stream function is only valid away from source and sink regions (i.e., the initial and final positions of particles), the small fraction of each connection that circulates south of Ouvéa Island has been deliberately omitted, without significant impact on the graphical representation of the contours. The full intensity of each connection is reported in Table 1. Panel c also shows the trajectory details for the fastest particles that travel from the Solomon Islands and reach Ouvéa Island in May 2011 (blue; 52.4 days), August 2011 (green; 61.4 days) and November 2011 (pink; 60.3 days). The diamond symbols sample the positions every 5 days, starting backward from the initial positions around Ouvéa Island. In panels a and b, only the fastest particle of each connection is shown (and corresponds in both cases to an arrival at Ouvéa Island in May 2011). (For interpretation of the references to color in this figure legend, the reader is referred to the web version of this article.)

**Table 1**
Fastest connection time and mean transport intensity for the three transfers to Ouvéa Island. The arrival dates around Ouvéa Island are distributed over 2011 and the length of the trajectories being considered is up to one year. The transport estimates use an arbitrary 10-m thickness for the surface layer.

| Geographical origin | Number of particles | Fastest connection (days) | Mean connection intensity ($m^2/s$) |
|---|---|---|---|
| Solomon Islands | 361 531 | 52.4 | 480 |
| Papua New Guinea | 129 202 | 76.8 | 170 |
| Gulf of Papua | 105 392 | 85.7 | 140 |

Ouvéa. We used the standard Ariane functionalities, adapted to a 2D time-varying velocity field. The vertical velocity was set to 0 and the surface currents were associated with a virtual 10-m-thick surface layer. The Lagrangian approach allows a full description of individual trajectories as well as volume transport estimates based on the small weights allotted to the numerical floats and assumed to be transported without alteration along its trajectory. The volume of water transported from an initial to a final geographical section is computed by summing the transport of the numerical floats that complete the pathway being considered (Döös, 1995). For each daily velocity sample over 2011, the initial particles were distributed around Ouvéa Island on the outer edge of the first belt of ocean grid cells (Fig. 4).

When directed toward the shore, the net transport across the face of a grid cell *Tr* (i.e., the value of the velocity times the thickness – 10 m – and cross-section of the corresponding grid cell) is divided up and distributed equally among $M^2$ particles regularly spaced along the grid cell faces perpendicular to the shore. The assignment of a vertical thickness to the cells satisfies the need of the Lagrangian toolkit to work with volume transports. While the choice of the vertical thickness seems arbitrary, it has no impact on the analysis due to internal normalizations. Unlike the standard 3D Ariane calculations (see Blanke et al., 1999), the calculations done here do not require a vertical distribution of the particles since the flow is assumed to be purely horizontal. The sum of all the transport weights divided by 365 is a measure of the average flow to Ouvéa Island in 2011. Increasing the number, *M*, of the particles increases the accuracy of the trajectories diagnosed by the backward Lagrangian integration. The value of M is adjusted locally so that the transport weight associated with each particle does not exceed a given threshold, $Tr_{max}$. Therefore, *M* is the smallest integer that satisfies $Tr/M^2 \leqslant Tr_{max}$. The calibration of $Tr_{max}$ is usually a trade-off between the computational burden and the desired accuracy of the results. Our experience from earlier work (e.g., Blanke et al., 2012) prompted us to adopt here $Tr_{max} = 5\ m^3/s$, which requires the use of 5,482,177 particles. Tests using a larger or smaller $Tr_{max}$, i.e., a lesser or greater number of particles, did not significantly alter the results, indicating the robustness of the analysis.

The particle paths were integrated backward in time until they intercepted control sections laid out around the Solomon Islands, around the southeastern tip of PNG and across the Gulf of Papua south of the Torres Strait, or until they recirculated back to the initial section around Ouvéa Island, for a maximum of 365 days. The following discussion focuses on the particles that successfully made the transect from the three remote origins and Ouvéa Island in less than one year.

## 3. Results

### 3.1. Pathways of the connections

The time-integrated transport field associated with the backward displacement of the particles initialized around Ouvéa Island can be portrayed by a Lagrangian stream function because the sources and sinks of volume are restricted to the arrival and departure islands with no loss of volume over the open ocean (Blanke et al., 1999). Temporal averaging smoothes out the smallest scales of variability associated with transient mesoscale and submesoscale features, and the contours of the stream function emphasize the most representative pathways. Fig. 5 shows the results obtained for the connections between Ouvéa and the Solomon Islands and between Ouvéa and the PNG coast. The number of contours in each plot is directly related to the intensity of the transfer under study (the contour interval is set to 10 $m^2/s$), and

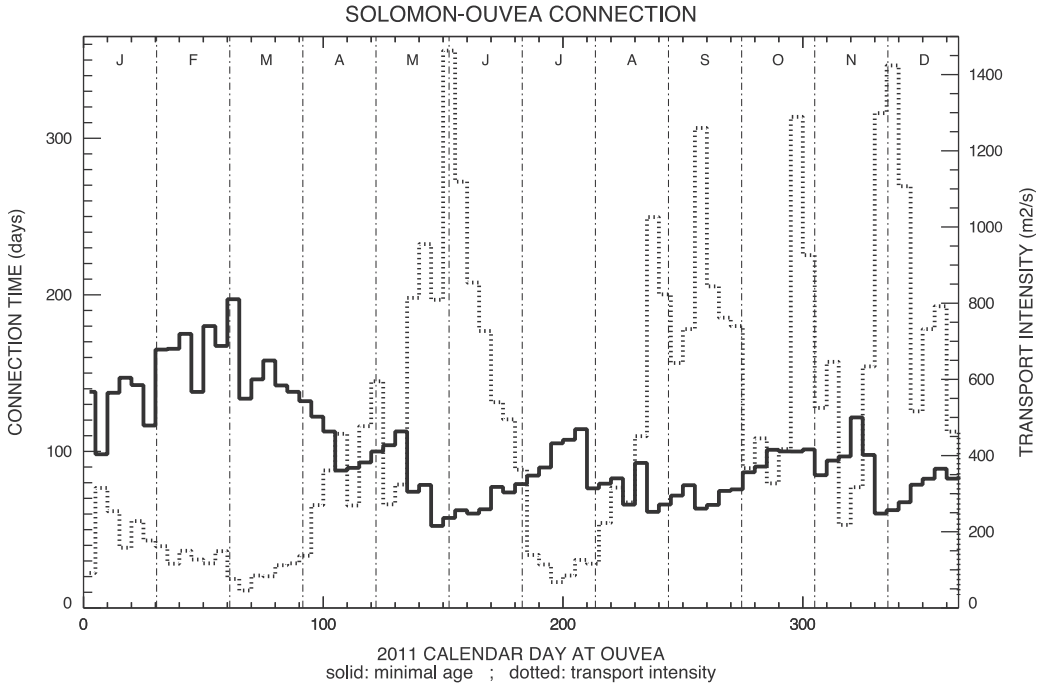


**Fig. 6.** Plots of the minimal age (solid line, in days) and transport intensity (dotted line, in $m^2/s$) for the connection achieved from the Solomon Islands to Ouvéa Island, as a function of the calendar day of 2011 for the initial positions around Ouvéa Island. The size of the bins used on the horizontal axis is 5 days.

the contours tighten along the routes favored by the individual particles.

South of 12°S, there is considerable similarity between the geometry of the three connections. Their intensities differ (Table 1), partly because the remote control sections that capture the backward trajectories did not have the same size (the Solomon Islands, for instance, had the largest meridional extension). On the other hand, the streamlines show the same approach to Ouvéa Island: the particles follow either a southeastward route roughly from 13°S to 160°E in the southeastern Coral Sea or a southward route between 165°E and 167°E along the Santa Cruz Islands and the Vanuatu Archipelago. North of 12°S, the three connections differ. The transfer from the Gulf of Papua (Fig. 5a) first follows the New Guinea Coastal Current (around 12°S) eastward until 155°E where it jogs south before continuing eastward in the northern Coral Sea, staying north of the westward flowing North Vanuatu Jet. It joins with the southern portion of the connection south of Rennel Island (around 12°S–160°E). The transfer from the southeastern tip of Papua New Guinea (Fig. 5b) is very similar, with the exception of its northernmost component that flows in the southern Solomon Sea, especially between Woodlark Island and Rossel Island. The connection from the Solomon Islands (Fig. 5c) mostly tracks south along the southwestern edge of the Archipelago, approaching the islands most closely at 156°E and 161°E. The eastern edge of the archipelago is associated with widely spaced contours of the stream function and corresponds to a clockwise route east of the Santa Cruz Islands, reaching as far east as the longitude of Fiji before turning southwestward and ultimately north and across the Vanuatu Islands.

Although this last connection is less energetic than the others, in the sense that the transit requires much more time than a direct path, it is worth noting that it bears many similarities to the trajectory of a surface drifter that was released during the SECARGO cruise in May 2010 between Vanuatu and the Solomon Islands (Fig. 1b in Reverdin et al., 2012).

Finally, the most important point to draw from these results is that they demonstrate the possibility of a southward surface transfer of mass from 10°S to 20°S despite the presence of two important westward jets: the North Vanuatu Jet (centered around 13°S) and the North Caledonia Jet (around 18°S).

### 3.2. Minimal connection times and calendar of stranding events

The shortest times needed to complete the connections can provide insight into the trajectories that fit best those of objects like the plastic bottles we found on the beach of Ouvéa Island. Individual fast trajectories can be superimposed on the contours of the stream functions to check visually whether the fastest particles follow specific paths or stretches of routes common to a large number of particles (see Fig. 5). Preferred stranding periods can be studied by considering the smallest connection times and the largest transport intensities. This is done by first partitioning the data into 5-day classes representing the sequence of arrival dates at Ouvéa Island. The shortest connection time of all the particles in each class was then plotted against the arrival date. Next the sum of the transport weights of the particles in each class was also plotted against the arrival date. The resulting combined plots are shown in Fig. 6 for the Solomon-Ouvéa connection.

Table 1 gives the minimal connection times obtained for all three transfers under study. Given the geometry of the connections, it is not surprising that the fastest particle originates in the Solomon Islands (with a journey slightly longer than 52 days). The connections from Papua New Guinea and the Gulf of Papua correspond to longer minimal times of about 77 and 86 days, respectively, because they also include eastward displacements in the northern Coral Sea and southern Solomon Sea.

Fig. 6 shows that the minimal time for the Solomon connection is obtained for an arrival in late May 2011 (on day 145) at Ouvéa Island indicating a departure from the Solomon Islands in early April 2011. Other short connection periods can be seen, especially at the end of August 2011 (61.4 days) and at the end of November 2011 (60.3 days). Note that the minimal connection time as a function of the day of arrival at Ouvéa Island has a phase nearly the opposite of the phase of the transport intensity. This result suggests that the variability of the circulation around Ouvéa Island is a key factor in determining the stranding time. The arrivals at Ouvéa occur in successive and irregularly spaced waves that integrate the fastest particles. If the regional circulation becomes weaker, then the transport intensity decreases and the ages of the particles increase. This phenomenon is confirmed by plots of the minimal connection times for the transfers from the Gulf of Papua and from Papua New Guinea (not shown): local minimal connection times are found on the same days at Ouvéa Island and the fastest connection time is also found in late May 2011.

The trajectories for the three fastest particles that travel from the Solomon Islands and reach Ouvéa Island in May, August and November 2011 are superimposed on the Lagrangian stream function in Fig. 5c. Unsurprisingly, the particles find their way across regions of tight contours of the Lagrangian stream function, which means that the shortest route is among those pathways followed by the greatest concentration of particles. The position of this pathway at the entrance to the Coral Sea is consistent with the fact that this region is singularly different from its western counterpart with regard to the persistent presence of Lagrangian Coherent Structures (LCS) as defined by Maes et al. (2013). LCSs organize the transport of the fluid properties such that they increase the residence time at sea of floating materials in contrast to more direct pathways which reduce the time at sea.

### 3.3. Comparison with actual drifter trajectories

The availability of actual surface drifter trajectories in the Coral Sea and Solomon Sea presented an opportunity to assess the soundness of the meridional displacements calculated from the

**Table 2**
Main characteristics of the 8 drifters found to cross (southward) the ocean box [155°E–170°E] [20°S–11°S]. The drifter ID refers to the AOML buoy identification number whereas the drifter label is used on Fig. 7 to identify each trajectory.

| Label | Drifter ID | Date at 11°S | Date at 20°S | Transit time (days) |
|---|---|---|---|---|
| 1 | 30471 | 10 June 2001, 06:00:00 | 26 Nov. 2001, 06:00:00 | 169.0 |
| 2 | 41092 | 19 Nov. 2010, 18:00:00 | 9 Apr. 2011, 18:00:00 | 141.0 |
| 3 | 2236921 | 31 Oct. 2003, 06:00:00 | 14 Feb. 2004, 12:00:00 | 106.2 |
| 4 | 7711045 | 11 May 1989, 12:00:00 | 13 Oct. 1989, 00:06:00 | 154.8 |
| 5 | 9217796 | 19 Aug. 1996, 00:00:00 | 26 Nov. 1996, 00:06:00 | 99.2 |
| 6 | 9423540 | 31 May 1996, 00:00:00 | 15 Aug. 1996, 00:00:00 | 76.0 |
| 7 | 9619652 | 20 Nov. 1999, 06:00:00 | 2 Mar. 2000, 00:00:00 | 102.8 |
| 8 | 9816379 | 1 Sep. 2000, 18:00:00 | 30 Oct. 2000, 18:00:00 | 59.2 |

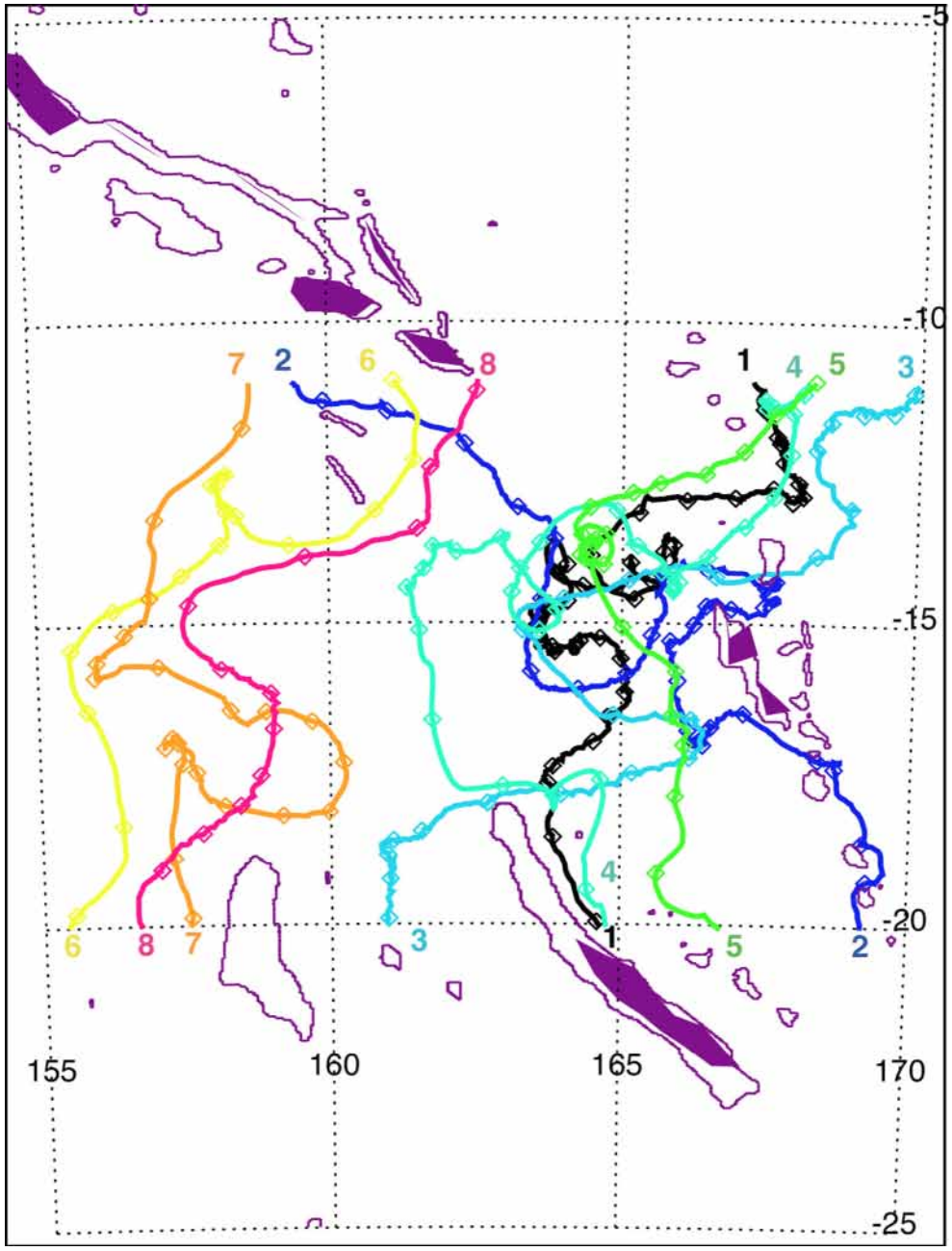


**Fig. 7.** Trajectory details for the 8 drifters of the AOML database found to cross (southward) the ocean box [155°E–170°E] [20°S–11°S]. See Table 1 for more information about these drifters. The diamond symbols sample the positions every 5 days (more precisely, at 00:00:00 and each time the Julian day modulo 5 evaluates to 0).

model velocity fields. We used the Atlantic Oceanographic and Meteorological Laboratory (AOML) portal to retrieve the trajectories of the drifters present in our area of study over 1979–2015. We then scanned the full set of positions and kept only the segments of trajectories that crossed the ocean box [155°E–170°E] [20°S–11°S] in the meridional direction. Only 8 drifters satisfied this condition, crossing it in the southward direction. The main characteristics of these drifters are summarized in Table 2 and their trajectories are shown in Fig. 7.

The number of available drifters was of course too small for a definitive validation of the meridional pathways diagnosed from the model between the Solomon Islands and Ouvéa Island, but some qualitative comments are possible. The field data confirm that such movements are not uncommon in the real ocean with time scales that are consistent with the age statistics shown in Fig. 6. The drifters labeled 2 and 8 deserve special attention because the duration of their trajectories in the region was short; they started near the Solomon Islands and they ended near land. Drifter 2 passed south of the Vanuatu Islands in April 2011 and eventually reached the Loyalty Islands a few weeks later in May 2011. A few months earlier, at the beginning of November 2010, this drifter had been very close to the Solomon Islands at around 155°E 8°S. Drifter 8 failed to approach Ouvéa Island but got close to the Chesterfield Archipelago with a traveling time from the southeastern tip of the Solomon Island (around 11°S–162.5°E) shorter than 60 days, which is comparable to the fastest connection times inferred from the model used in this study. This result gives some credence to the surface circulation simulated by the model and to the diagnosed Lagrangian dispersion and pathways determined with Ariane.

## 4. Concluding remarks

The calculation of the kinetic energy of the NLOM velocity field shows that the Coral Sea (as elsewhere across the World's ocean) is dominated by small-scale dynamics. In this study, we used a Lagrangian interpretation of a model output that includes submesoscale structures such as very small eddies, filaments and fronts. This choice was suggested by an earlier study that showed that transfer times in the surface layers of the ocean are highly sensitive to the smallest details of the velocity field (Blanke et al., 2012). In addition to the calculations described in this paper we also examined the output of a global eddy-permitting ocean model experiment run at coarser 1/4° horizontal resolution and driven by realistic atmospheric forcing over 1958–2012 period. Although the general organization of the transport field (not shown) was rather similar to that in Fig. 5, the minimal times needed for the connections to complete were much larger, by a factor of 2 or more. These results demonstrate the value of integral transfer times diagnosed from the release and collection of floating markers in high-resolution ocean models in making sense of the distribution of floating materials, whether the result of careless littering or the result of a carefully controlled deployment of drifters for scientific research.

The presence of plastics in the oceans and their impact on the whole biosphere has as its root cause the massive human production of single-use, disposable plastic items. This crisis will likely remain a global environmental issue for several decades to come, owing to the difficulty in establishing any kind of international regulation and enforcement, especially in remote and low population regions (Gregory, 1999). The goal of this study was not to point a finger at any likely source for the release of this litter. Rather, our investigation shows that when the origins and pathways of trash can be established, it represents valuable information that can be used to test and, ultimately, improve our understanding of ocean circulation. Our expectation is that such information is central to solving scientific problems such as the dispersal of marine populations and species (including complex coral reef ecosystems). It is in understanding their connectivity over long distances, that we will be able to set up and to develop effective conservation and management programs.

## Acknowledgements

Our study benefited from different data sets that are freely available on the Internet. This includes the NLOM outputs from APDRC (http://apdrc.soest.hawaii.edu/data/), the delayed-time geostrophic velocities from AVISO (http://motu.aviso.oceanobs.com/aviso-gateway-servlet/Motu?action=listcatalog&service=AvisoDT) and the surface drifters from AOML (http://www.aoml.noaa.gov/envids/gld/dirkrig/parttrk_spatial_temporal.php). The detailed map of the Ouvéa Island has been provided by Eric Opigez from IRD France Nord. We are grateful to the teams and ship crews who made possible the various in situ measurements during the oceanographic cruises identified in this study. Measurements of microplastics in the samples collected during the Bifurcation cruise have been done by Maryvonne Henry and Francois Galgani. Fruitful discussions and exchanges on surface drifters with Dr Rick Lumpkin and Dr Les Hamilton are gratefully acknowledged. Comments from Dr Elodie Martinez and Dr Andréa Doglioli have been greatly appreciated and we address a special thank to Dave Berhinger for his patient work on the original manuscript. We wish also to thank Ms Abla Atsamnia for her help during the collection of the plastic bottles on the Ouvéa beach.

## References

Arakawa, A. (1972), Design of the UCLA general circulation model, Numerical simulation of weather and climate. Tech. Rep. 7, Dept. of Meteorology, University of California, Los Angeles, p. 116.

Bailly du Bois, P., Garreau, P., Laguionie, P., Korsakissok, I., 2014. Comparison between modelling and measurement of marine dispersion, environmental half-time and 137Cs inventories after the Fukushima Daiichi accident. Ocean Dyn. 64 (3), 361–383. http://dx.doi.org/10.1007/s10236-013-0682-5.

Blanke, B., Raynaud, S., 1997. Kinematics of the pacific equatorial undercurrent : An Eulerian and Lagrangian approach from GCM results. J. Phys. Oceanogr. 27, 1038–1053.

Blanke, B., Arhan, M., Madec, G., Roche, S., 1999. Warm water paths in the equatorial Atlantic as diagnosed with a general circulation model. J. Phys. Oceanogr. 29, 2753–2768.

Blanke, B., Bonhommeau, S., Grima, N., Drillet, Y., 2012. Sensitivity of advective transfer times across the North Atlantic Ocean to the temporal and spatial resolution of model velocity data: Implication for European eel larval transport. Dyn. Atmos. Oceans 55–56, 22–44.

Carpenter, E.J., Smith Jr., K.L., 1972. Plastics on the Sargasso Sea surface. Science 175, 1240–1241.

Choukroun, S., Ridd, P.V., Brinkman, R., McKinna, L.I.W., 2010. On the surface circulation in the western Coral Sea and residence times in the Great Barrier Reef. J. Geophys. Res. 115, C06013. http://dx.doi.org/10.1029/2009JC005761.

Cravatte, S., Ganachaud, A., Duong, Q., Kessler, W.S., Eldin, G., Dutrieux, P., 2011. Observed circulation in the Solomon Sea from SADCP data. Prog. Oceanogr. 88, 116–130.

Depledge, M.H., Galgani, F., Panti, C., Caliani, I., Casini, S., Fossi, M.C., 2013. Plastic litter in the sea. Mar. Environ. Res. 92, 279–281. http://dx.doi.org/10.1016/j.marenvres.2013.10.002.

Dohan, K., Maximenko, N., 2010. Monitoring ocean currents with satellite sensors. Oceanography 23, 94–103. http://dx.doi.org/10.5670/oceanog.2010.08.

Döös, K., 1995. Interocean exchange of water masses in the southern ocean. J. Geophys. Res. 100, 13499–13514.

Eriksen, M., Lebreton, L.C.M., Carson, H.S., Thiel, M., Moore, C.J., Borerro, J.C., Galgani, F., Ryan, P.G., Reisser, J., 2014. Plastic pollution in the World's oceans: More than 5 trillion plastic pieces weighing over 250,000 tons afloat at sea. PLoS ONE 9 (12), e111913. http://dx.doi.org/10.1371/journal.pone.0111913.

Froyland, G., Stuart, R.M., van Sebille, E., 2014. How well-connected is the surface of the global ocean? Chaos 24, 033126. http://dx.doi.org/10.1063/1.4892530.

Ganachaud, A. et al., 2014. The Southwest Pacific Ocean circulation and climate experiment (SPICE). J. Geophys. Res.-Oceans 119, 7660–7686. http://dx.doi.org/10.1002/2013JC009678.

Gasparin, F., Ganachaud, A., Maes, C., Marin, F., Eldin, G., 2012. Oceanic transports through the Solomon sea: The bend of the New Guinea coastal undercurrent. Geophys. Res. Lett. 39, L15608. http://dx.doi.org/10.1029/2012GL052575.

Gregory, M.R., 1999. Plastics and South Pacific island shores. Ocean Coast. Manag. 42, 603–615. http://dx.doi.org/10.1016/S0964-5691(99)00036-8.

Hristova, H.G., Kessler, W.S., 2012. Surface circulation in the Solomon Sea derived from Lagrangian drifter observations. J. Phys. Oceanogr. 42, 448–458.

Kessler, W.S., Gourdeau, L., 2007. The annual cycle of circulation of the Southwest Subtropical Pacific, analyzed in an Ocean GCM. J. Phys. Oceanogr. 37, 1610–1627. http://dx.doi.org/10.1175/JPO3046.1.

Maes, C., Dewitte, B., Sudre, J., Garcon, V., Varillon, D., 2013. Small-scale features of temperature and salinity surface fields in the Coral Sea. J. Geophys. Res. Oceans 118, 5426–5438. http://dx.doi.org/10.1002/jgrc.20344.

Martinez, E., Maamaatuaiahutapu, K., Taillandier, V., 2009. Floating marine debris surface drift: convergence and accumulation toward the South Pacific subtropical gyre. Mar. Pollut. Bull. 58, 1347–1355.

Maximenko, N.A., Hafner, J., Niiler, P.P., 2012. Pathways of marine debris derived from trajectories of Lagrangian drifters. Mar. Pollut. Bull. 65, 51–62.

Reverdin, G., Morisset, S., Boutin, J., Martin, N., 2012. Rain-induced variability of near sea-surface T and S from drifter data. J. Geophys. Res. Oceans 117, C02032. http://dx.doi.org/10.1029/2011JC007549.

Shriver, J.F., Hurlburt, H.E., Smedstad, O.M., Wallcraft, A.J., Rhodes, R.C., 2007. 1/32° real-time global ocean prediction and value-added over 1/16° resolution. J. Mar. Syst. 65, 3–26.

Sudre, J., Maes, C., Garcon, V., 2013. On the global estimates of geostrophic and Ekman surface currents. Limnol. Oceanogr.: Fluids Environ. 3, 1–20. http://dx.doi.org/10.1215/21573689-2071927.

Webb, D.J., 2000. Evidence for shallow zonal jets in the South Equatorial Current region of the southwest Pacific. J. Phys. Oceanogr. 30, 706–719.